Radiation Environment in MARS End Cells

Laila A. El-Guebaly

October 1984

UWFDM-596

FUSION TECHNOLOGY INSTITUTE

UNIVERSITY OF WISCONSIN

MADISON WISCONSIN

Radiation Environment in MARS End Cells

Laila A. El-Guebaly

Fusion Technology Institute
University of Wisconsin
1500 Engineering Drive
Madison, WI 53706

http://fti.neep.wisc.edu

October 1984

UWFDM-596

RADIATION ENVIRONMENT IN MARS END CELLS

Laila A. El-Guebaly

Fusion Technology Institute
University of Wisconsin-Madison
1500 Johnson Drive
Madison, Wisconsin 53706

October 1984

UWFDM-596

Table of Contents

		Page
1.	Introduction	1
2.	End Cell Streaming Analysis	5
	2.1 Calculational Model	5
	2.2 Calculational Procedures and Results	8
3.	Radiation Analyses of the NBI	15
	3.1 General Features	15
	3.2 Study Goals	19
	3.3 Design Considerations	20
	3.4 Penetration Shield Design	23
	3.5 Calculational Procedures and Results	24
4.	Radiation Analyses for the Direct Convertor	28
	4.1 Neutronics Analyses	31
	4.2 Activation Analyses	33
5.	Conclusions	36
References		38

1. INTRODUCTION

In recent studies of tandem mirror reactors some attention has been focused on the problems associated with radiation streaming into penetrations of both the central fusion chamber and the end cells. The problem of radiation in penetrations has been recognized for some time in tokamak studies. In a tandem mirror power reactor design the problem appears to be less severe since the only penetrations of the central fusion chamber are the openings to the end cells. Fortunately, in most TMR designs the end cell penetrations are not in direct line of sight of the central cell source neutrons. Hence, the neutron source in the end cell dominates the streaming problem and the problem of neutron streaming from the central cell to the end cell only concerns the leakage to the ends of the reactor where the direct convertors are located. Considerable amounts of neutrons are generated in the end cells and the streaming of these neutrons through the penetrations reduces the effectiveness of the bulk shield and presents a variety of shielding and maintenance problems to the designers as the sensitive components located at the back of these penetrations are subject to damage by radiation. Substantial work[1-5] during the past ten years uncovered the severity of the penetration problems. Some problems can be solved by introducing a radiation shield and extending it to the back of the penetration to protect the various components, but the main constraints could be the space limitations and the interference of the shield with a desirable arrangement of the components.

In this study, the radiation analysis was carried out for the end cells of the commercial tandem mirror reactor MARS.[6,7] An overview drawing showing the main components of the reactor is given in Fig. 1. The 130 m long central cell produces 2600 MW of fusion power in steady state and has a neutron wall

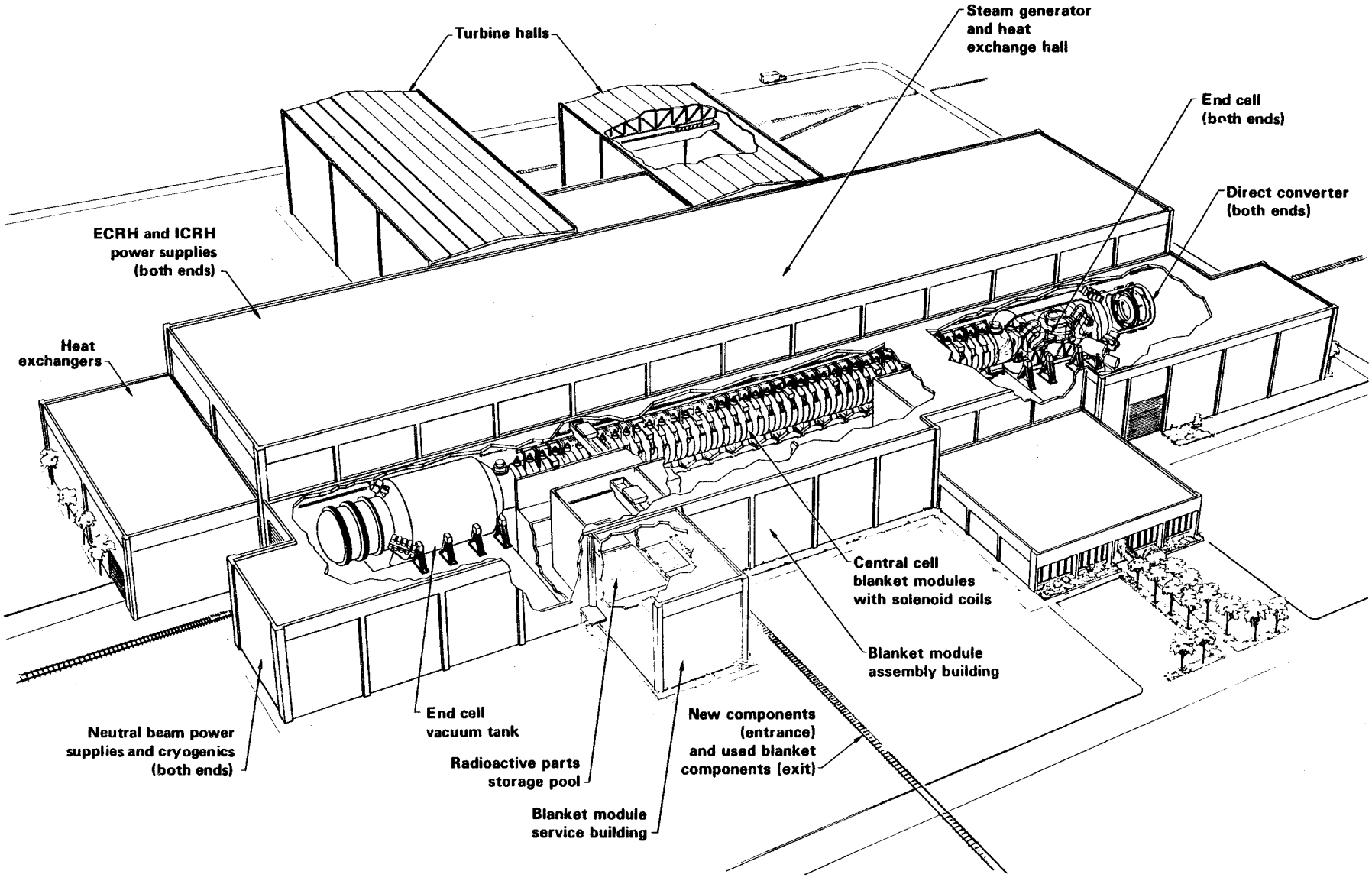

Fig. 1 Overview of the MARS tandem mirror reactor.

loading of 4.3 MW/m^2. Other features include the use of HT-9 for structural material and $Li_{17}Pb_{83}$ as the breeder and coolant. There is a high field choke coil at each end of the central cell, followed by a series of six C-shaped coils (Fig. 2). Small copper insert coils (0.6 m bore) are used to boost the choke coil fields to 24 T. The direct conversion of the energy of the particles which leak out of both ends of the machine is accomplished by compact, gridless direct convertors which supply all the plant auxiliary power. The end cell (40 m long) includes the transition, anchor, plug, recircularizer, and direct convertor regions. It consists of the C coils and their shield and support structure, penetrations for the neutral beam injector (NBI) and ion and electron cyclotron resonance heating (ICRH and ECRH), neutral beam dumps, and the ion and electron thermal dumps at the direct convertor collector plates.

The general objectives of this study are to 1) analyze the streaming problems in the end cell, 2) provide radiation sources at the penetration entrances to be used in later modeling of the ducts themselves, 3) model the penetration with the most severe nuclear environment for radiation analyses, and 4) investigate the possibility of simple disposal of radioactive waste of the direct convertor collector plates. The modeling of the end cell shield configuration and the various penetrations for the three-dimensional Monte Carlo code and the resulting radiation streaming into the penetrations are presented in Section 2. Section 3 covers the modeling of the NBI and the calculational features of this problem. The calculations of the neutron flux at the direct convertor collector plates as a result of streaming neutrons from the reaction chamber are discussed in Section 4 along with the subsequent activation analyses of these plates. Finally, the conclusions to be drawn

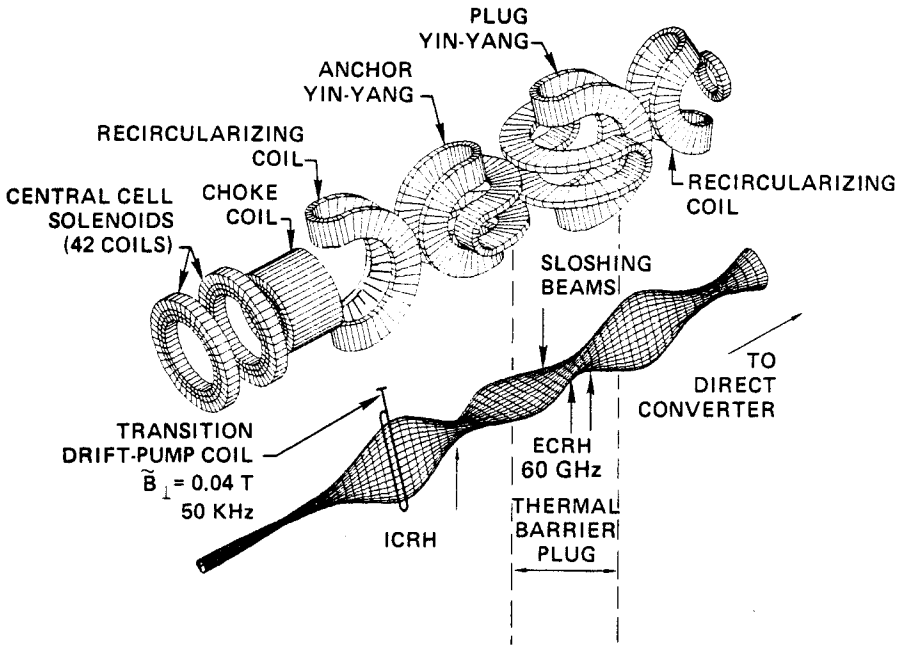

Fig. 2 The magnet arrangement and the plasma flux tube in the end cell of MARS.

from this work are discussed in Section 5. It should be mentioned that brief descriptions of some related topics are given in each section and the reader should refer to the main report[6] for more thorough coverage.

2. END CELL STREAMING ANALYSIS

Our interest here is centered on the radiation streaming through the end cell penetrations. This is of great importance in assessing the radiation effects in these penetrations. Evaluation of the radiation streaming through the ducts requires an accurate knowledge of the neutron source and the geometrical configuration of the shield as well as the size of the ducts. The linear neutron source distribution from the midplane of the choke coils to the end of the machine is shown in Fig. 3 along with the axial variation of the peak neutron wall loading. They are characterized by two relative peaks which drop to a negligible value near the end of the plug region. Figure 4 illustrates the end cell shield wall which closely follows the plasma boundary and allows for the required spacing for the halo region. The plasma is circular in cross section up to the midplane of the choke coils and has an elliptical shape with varying ellipticity in the end cell. From the parametric study of the end cell shielding materials, the Fe1422/B_4C/H_2O shield was dictated as the best for meeting the combined criteria of low cost and adequate magnet protection. The ~ 0.5 m thick shield used in the end cell results in acceptable values for the damage in the C coils.

2.1 Calculational Model

To deal with the three-dimensional (3-D) geometrical configuration of the shield, the Monte Carlo code MCNP[8] and its RMCCS cross section library were

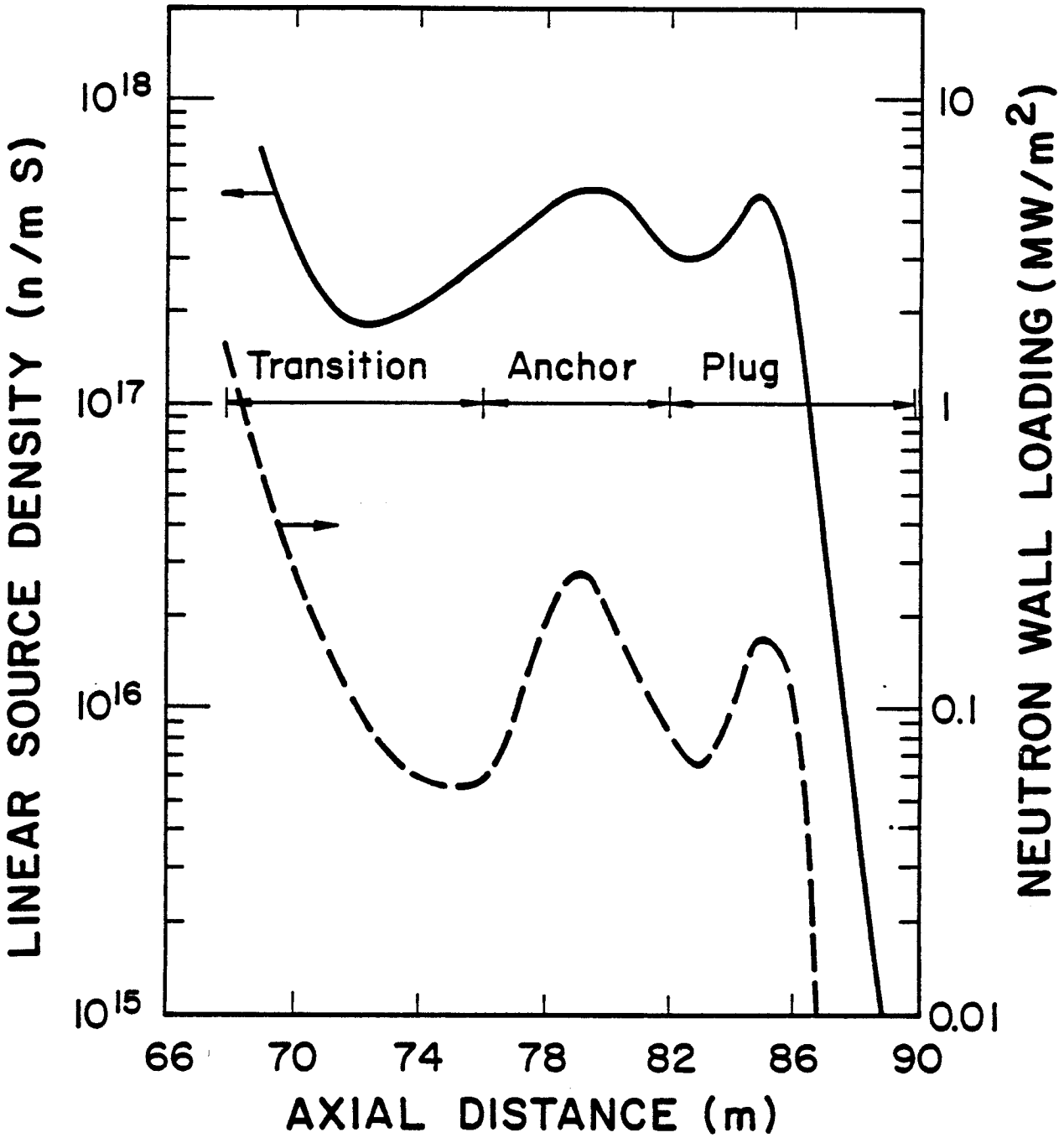

Fig. 3 Axial variation of the neutron source strength and wall loading in the end cell (the axial distance is measured from the midplane of the reactor).

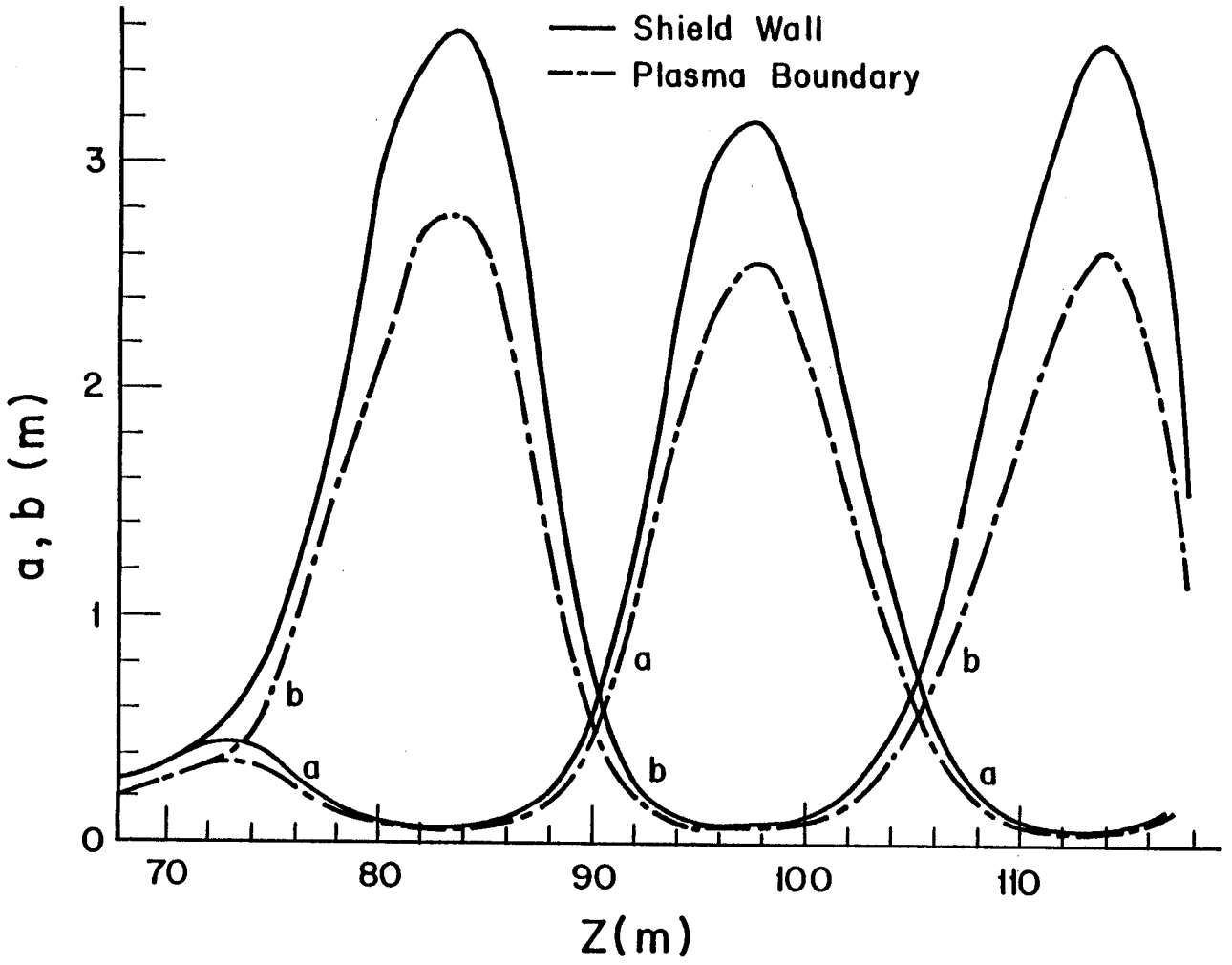

Fig. 4 Axial variation of the elliptical plasma surface and first wall semi-diameters a and b.

used for the treatment of the streaming problem. The end cell shield and penetrations were modeled for the code and an effort was made to minimize the geometrical approximations of the shield. Figure 5 shows elevation and plan views of the model from the midplane of the choke coils to the end of the reactor. The figure is an output from the MCNP plotting routine and illustrates the geometrical relationship of the ducts to the reactor. The axial locations and the sizes of the various penetrations are given in detail in Table 1. The plasma boundary is not shown in the figure and the vertical lines are only used to define the regions for the code. Nominally, 0.5 m of shield is used in the end cell except at z positions in the range 88.35 - 92.35 m where the shield thickness is reduced to allow for the 0.64 m wide ECRH(B) ducts. There are no source neutrons in the recirculariser region. Nevertheless, a ~ 0.2 m thick shield is placed there to shield the plug-Yang and recirculariser coils against the streaming radiation from the reaction chamber.

2.2 Calculational Procedures and Results

The model shown in Fig. 5 was entered into the MCNP input to perform the 3-D neutronics and photonics calculations of the streaming problem. Trapping surfaces were located at the duct entrance surfaces* to count all crossing particles according to angle and energy bins. This information was then stored to serve as surface sources in later modeling of the ducts themselves.

*For the ECRH ducts, where the entrances consist of the intersection of several surfaces, the trapping surfaces are located behind the duct entrances.

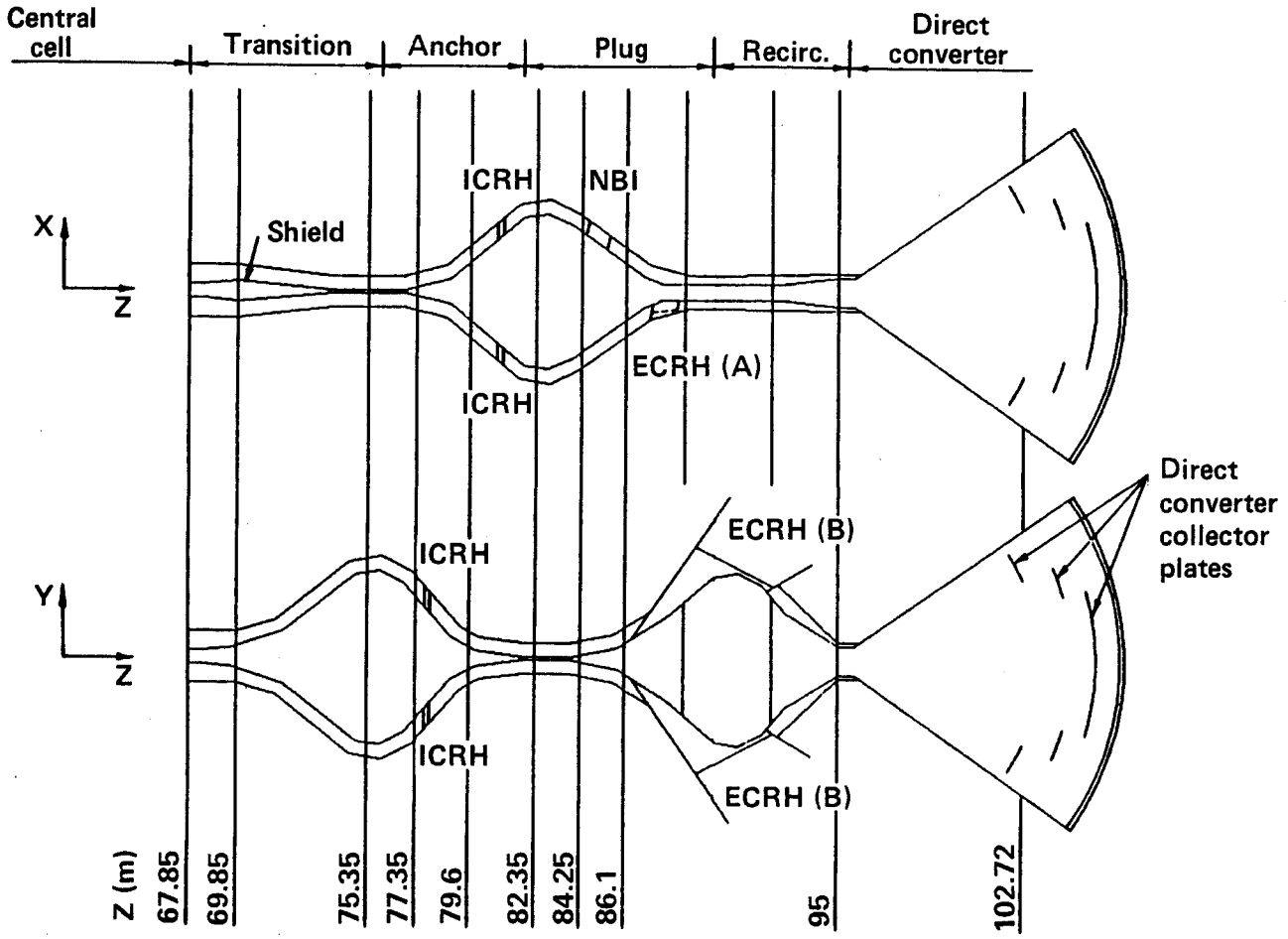

Fig. 5 Elevation and plan views of MARS end cell shield.

Table 1. End cell penetrations.

Duct	# per end	Location	Z* (m)	Size (m)	Injection angle**
NBI	1	Plug	84.35	0.8 x 0.3	76°
ICRH	4	Anchor	77.85, 80.85	.232 dia.	90°
ECRH (B)	2	Plug	85.85 - 87.35	1.5 x 0.64 (at z axis)	55° - 31°
ECRH (A)	1	Plug	88.37 - 89.33	0.96 x 0.64	74° - 81°

*Intersection of the beam centerline with the plasma axis except for ECRH where the duct wall intersection is given.

**Measured from the plasma axis.

The end cell penetrations are not in direct line of sight of the central cell source neutrons. Hence, the neutron source in the end cell dominates the streaming problem. A run of 50,000 histories was sampled isotropically from axial positions in the range 67.85 m to 90 m, according to the actual plasma shape (Fig. 4) and axial neutron source distribution (Fig. 3). Normalization of the source was such as to represent a neutron source of 7×10^{18} n/s. This source corresponds to a fusion power of 19.7 MW (at 17.6 MeV/fusion) for each end cell.

The number of particles crossing each trapping surface is given in Table 2 on a per second basis along with their associated relative standard deviations that range from 7 to 17% for neutrons and 20 to 61% for gamma rays. The NBI duct is the most severe case as is evident by observation of the energy current density in the right hand column of the tabulated results. The energy spectra and angular distributions for particles crossing the NBI trapping surface are presented in Figs. 6 and 7. The energy spectra show that approximately 24% of the crossing neutrons are source neutrons at 14.1 MeV. A significant number of lower energy secondary neutrons that have been moderated in and reflected from the shield also stream through the duct, and ~ 70% of the neutrons have energies below 1.35 MeV. The angular distribution abscissa, labeled cosine (theta), represents the cosine of the angle that the particle makes with the normal to the trapping surface. Inspection of the figure reveals that the angular distribution of the particles peaks at normal incidence and most particles stream along the beam line. This serves as a warning to carefully shield the NBI system in order to protect the vital components located at the back of the injector.

Table 2. Radiation streaming through end cell penetrations.

Duct*	Duct opening area (m^2)	Neutron/s	Gamma/s	Energy current density (MW/m^2)
NBI	0.24	2.204×10^{16}(±7%)	3.750×10^{15}(±20%)	6.194×10^{-2}
ECRH (A)	0.71	1.544×10^{16}(±9%)	2.564×10^{15}(±30%)	1.015×10^{-2}
ECRH (B-)	2.33	4.396×10^{15}(±17%)	5.60×10^{14}(±50%)	1.472×10^{-3}
ECRH (B+)	2.33	3.887×10^{15}(±17%)	7.761×10^{14}(±53%)	1.306×10^{-3}
ICRH (+x)	4.28×10^{-2}	6.398×10^{15}(±14%)	1.469×10^{15}(±37%)	7.665×10^{-2}
ICRH (-x)	4.28×10^{-2}	5.524×10^{15}(±15%)	6.124×10^{14}(±61%)	7.286×10^{-2}
ICRH (+y)	4.28×10^{-2}	6.378×10^{15}(±14%)	1.319×10^{15}(±39%)	8.977×10^{-2}
ICRH (-y)	4.28×10^{-2}	5.232×10^{15}(±15%)	1.755×10^{15}(±38%)	7.724×10^{-2}

*(+x) means duct at the positive x axis.

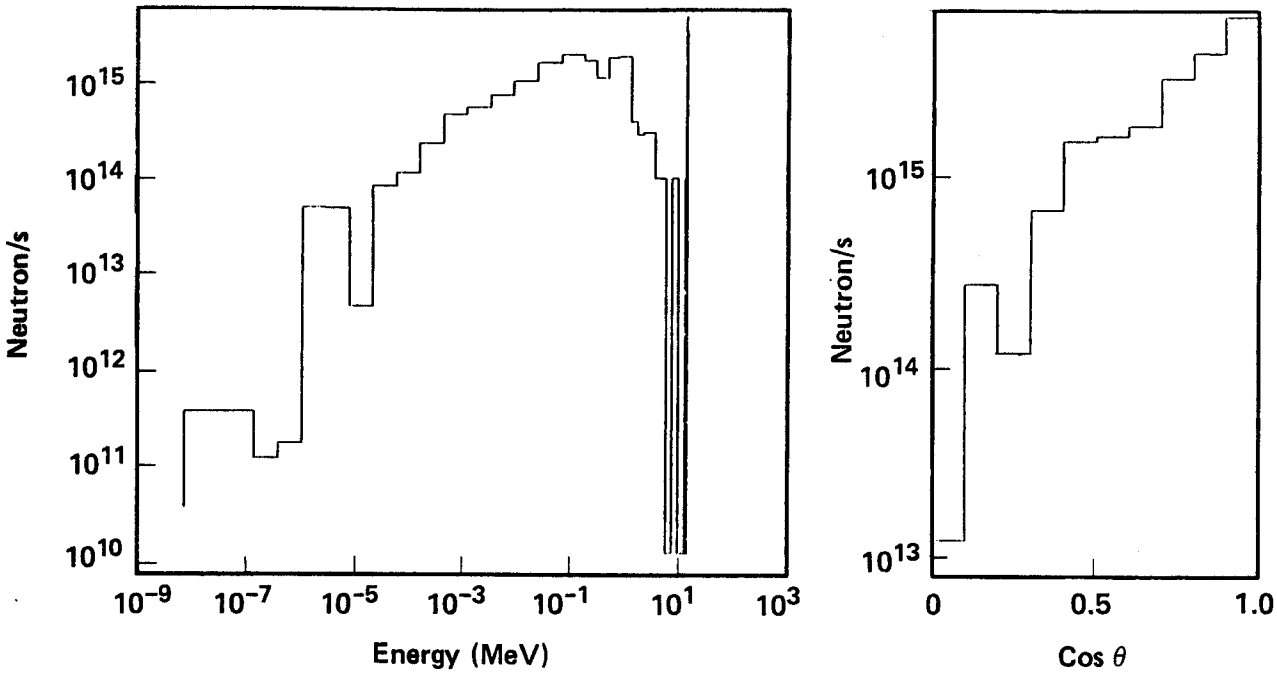

Fig. 6 Energy spectrum and angular distribution of neutrons streaming through the NBI duct.

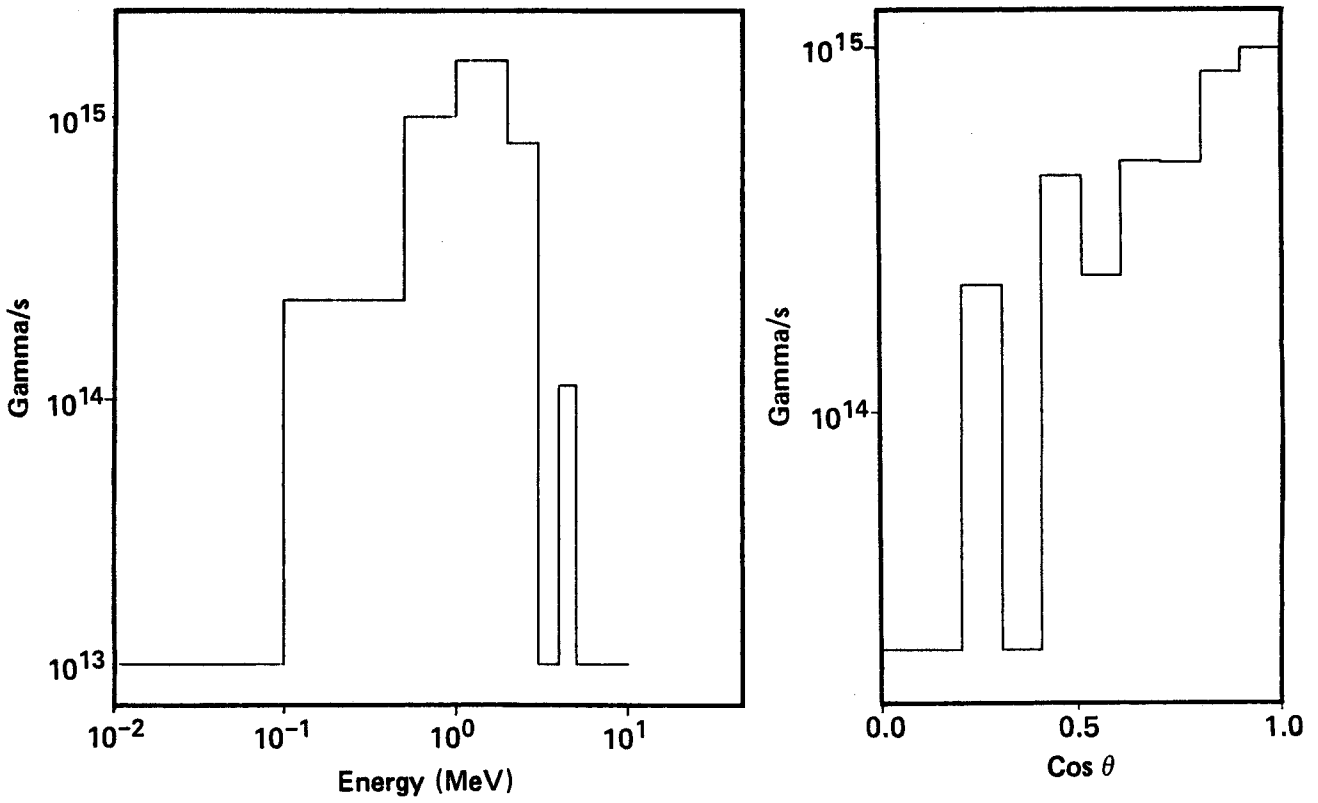

Fig. 7 Energy spectrum and angular distribution of gamma rays streaming through the NBI duct.

3. RADIATION ANALYSES OF THE NBI SYSTEM

3.1 General Features

The end cell requires a number of heating systems to produce the necessary potential, pressure, and density profile that ensure stability, confinement, and overall desirable operating characteristics. The heating systems include the ECRH, ICRH, and the high energy neutral beam system. The NBI was selected for radiation analyses as it has the largest streaming radiation among the MARS end cell penetrations (see Table 1). Radiation effects in the other systems also need to be analyzed, although the problems seem to be less severe, particularly in the ECRH system. This was accomplished by moving the launcher far from the neutron source, using a quasi-optical transmission system, and by placing the gyrotrons behind a radiation shield.

Recently, the acceptability of NBI heating based on positive-ion sources for fusion reactors has been seriously questioned because of the engineering complications and the low overall efficiency of this scheme. On the other hand, NBI heating based on negative-ion beams is an area in which recent advances improve the prospects for a system with high efficiency and significantly reduced neutron streaming. Radiation streaming through the NBI duct introduces significant problems in the operation and maintenance of the critical components of the system. An attractive and practical solution is to provide several bends in the penetrations and strong transport structures capable of transporting the heating particles around the bends in channels through the penetration shield. This option has proven to provide effective attenuation for the streaming radiation.[4,5] These combined factors dictated the choice of the Berkeley version as the baseline design for the MARS sloshing ion beam line. One important achievement is the installation of the ion

sources and the high-voltage sections in a low neutron environment off the direct line of sight of the streaming radiation by employing a rather long and curved beam transport system penetrating the shield, thus adding to the reliability, reducing radiation damage and simplifying maintenance of the vital components.

The NBI is required to deliver a total of 14.75 A at 475 keV and is based on negative ions which can be efficiently converted to neutrals at such high energy. Figure 8 shows schematically the main components of the sloshing ion beam line. Multiple sources in each beam line form ribbon beams for the accelerator. The LBL (Lawrence Berkeley Laboratory) self-extraction negative ion sources,[9,10] shown in Fig. 9, produce negative ions on the surface of a cesiated electrode in contact with a deuterium plasma. The source ions are pre-accelerated to 80 keV by a standard DC multiple grid set before being injected into a four stage Transverse Field Focussing (TFF) accelerator. The TFF system uses transverse electrostatic fields alternating in direction to focus and control the beam. It consists of properly shaped and oriented grids that offer the possibility of bending the ribbon beam with a short enough radius (~ 0.4 m) that the beam can be transported through a sinuous path of reasonable length surrounded by shield to greatly attenuate the streaming radiation through the NBI duct and alleviate problems of activation of the ion sources and accelerators. The accelerated negative ions are converted to neutral atoms by passing the ion beam through a folded resonator laser photodetachment neutralizer; a conversion efficiency of 95% or more is possible. The beam then passes through a sweep magnet where the remaining ions are removed from the neutral beam. A considerable amount of this ion energy is recovered by the ion-beam dump. The cryopumps distributed along the beam line

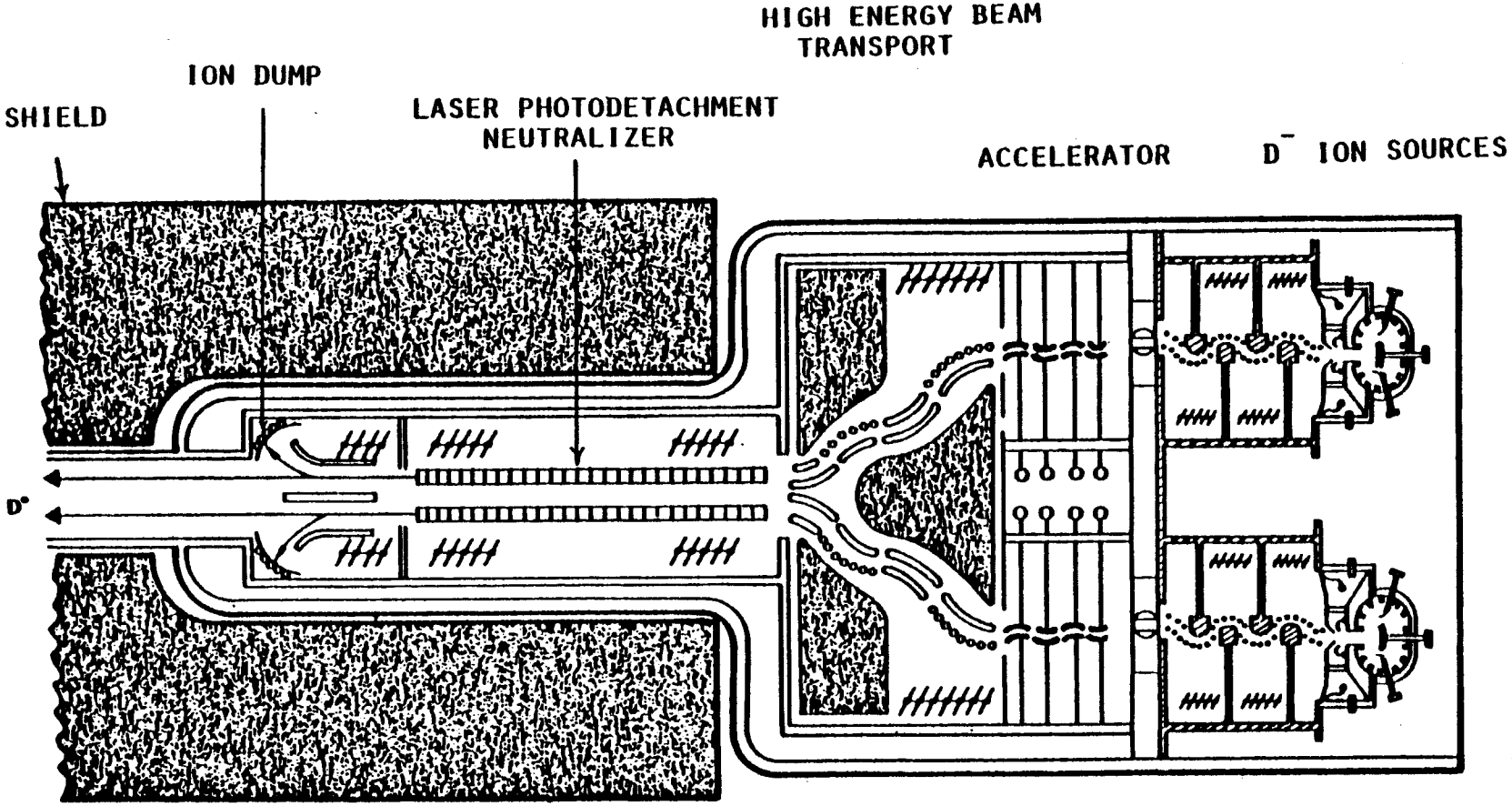

Fig. 8 Schematic of MARS sloshing ion beam line (the neutralizers are shown only for clarity).

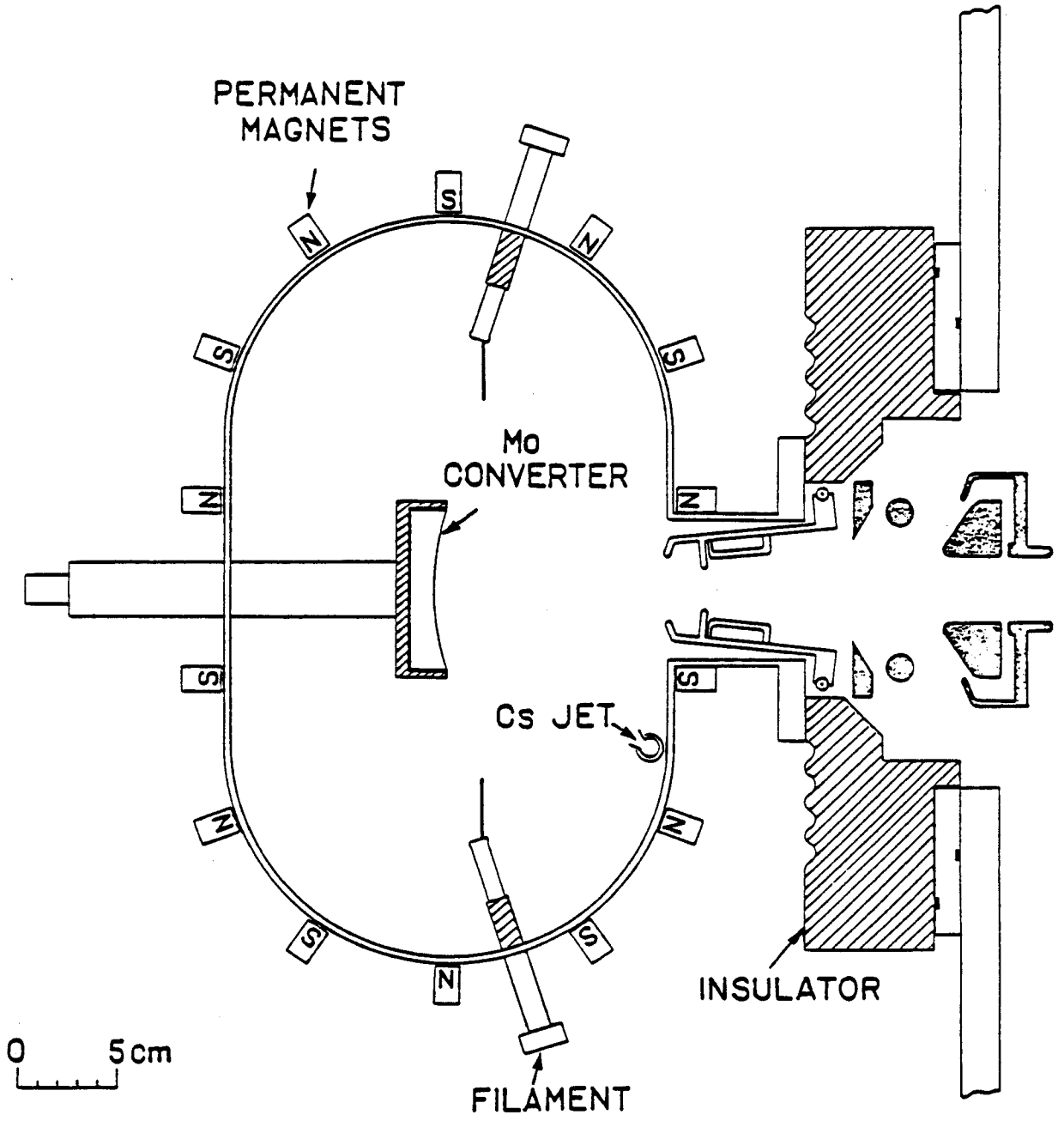

Fig. 9 The LBL self-extraction negative ion source.

remove most of the gases emerging from the neutralizer and the ion-beam dumps, and maintain the pressure at a sufficiently low value so that very little of the neutral beam is reionized.

3.2 Study Goals

The aim of this study is to design a suitable radiation shield for the NBI, select low activation materials for the different components, evaluate the radiation effects on the high voltage insulators, the nuclear heat loads on the cryopanels and magnetic shield, the heating effects for the laser neutralizer mirrors, and calculate the biological dose rate at the back of the injector where hands-on maintenance is highly desirable. Until recently, it was assumed that the injector would become activated by the streaming neutrons and that the maintenance must be by remote procedures. The new concept of hands-on maintenance of the injector has been brought on by a better design and off-axis arrangement for the most sensitive components of the NBI. The criterion for hands-on maintenance is to have a dose rate not greater than 2.5 mrem/h at the end of a cooling-off period of 48 hours after reactor shutdown to be able to maintain the ion sources without a special radiation shield. To assess the feasibility of hands-on maintenance, detailed 3-D neutronics calculations are required to compute the neutron flux at the various components of the NBI. These are followed by activation analyses to produce the decay gamma ray sources at the end of a one full power year (FPY) irradiation period. Then, 3-D gamma transport calculations are performed and the dose is determined two days after shutdown at various locations outside the NBI.

3.3 Design Considerations

The NBI was modeled for the Monte Carlo code MCNP.[8] Figure 10 shows vertical and horizontal planes for the NBI and the 18 regions of the NBI are identified by Table 3. Due to symmetry, one-fourth of the NBI was modeled with reflecting boundaries at the injector axis. Only those components which have significant effects on the activation of the ion sources are included in reasonable detail. The high energy beam transport (HEBT) consists of two TFF stages, each with a right angle bend and 0.4 m radius of curvature. The transverse spacing between the 0.01 m thick electrodes is 0.04 m.

To keep the radiation around the NBI to reasonable levels, the materials and thicknesses of the components (Table 3) were chosen based on activation considerations while meeting the structural and functional demands. In general, the use of copper was avoided and the HT-9 structural material is used in the hard neutron spectrum region of the straight beam duct (starting from the injector entrance up to the beginning of the HEBT section). In this region the use of Al was excluded to avoid the production of ^{24}Na by the energetic neutrons[11] (E > 5 MeV). In the accelerator region, where the neutron spectrum is relatively soft, Al is preferable[11]. The electrodes are chosen as thin as possible as well as their supports to meet the activation constraints. The 304-SS steel alloy is less activated[12] than Fe1422 steel. Accordingly, the 304-SS was selected as the structural material of the NBI penetration shield. Even though the HT-9 would be less activated[12] than 304-SS, its well known DBTT problem at low temperatures characteristic of the water cooled shield has led to its exclusion. Although $SmCo_5$ is a highly radioactive material, it is used in the permanent magnets of the ion source, shown in Fig. 9, as no other candidate material can produce the required high

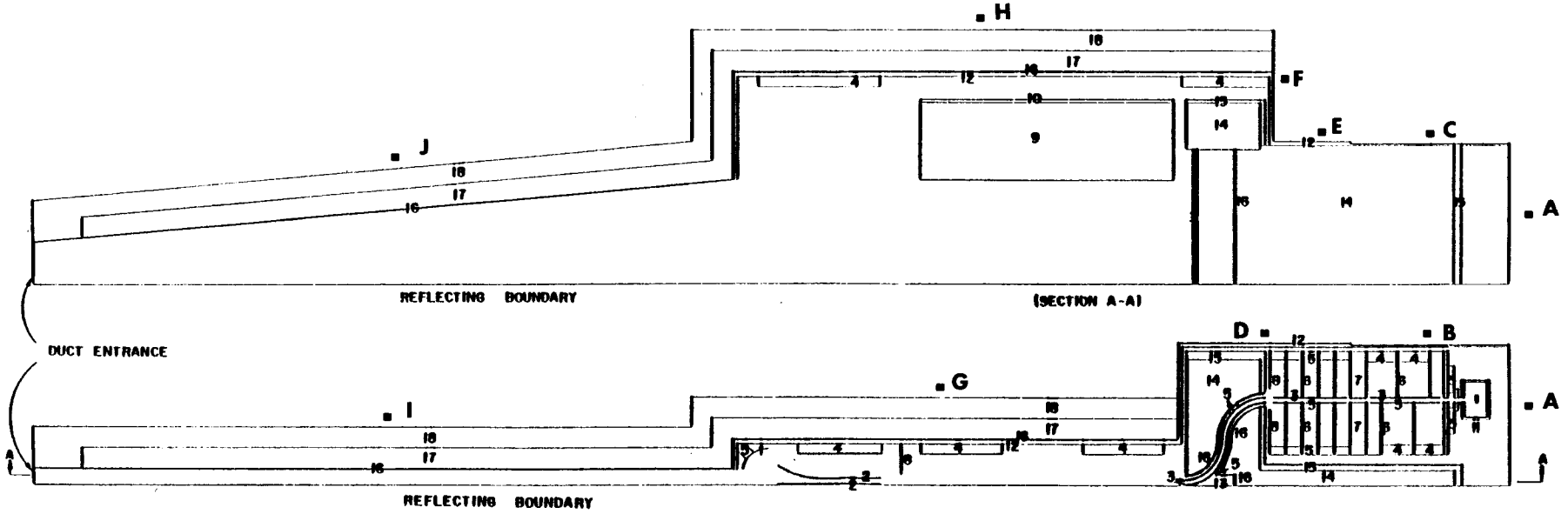

Fig. 10 Vertical and horizontal cross sections of the NBI (output from MCNP plotting routine); numbers on the figure are for the regions identified in Table 3.

Table 3. Dimensions and compositions of the material zones in the NBI.

Region	Identification	Dimension (m)	Material
1	ion dump	0.06 thick	Al
2	electrostatic plates	0.01 x 1 x 1.1	HT-9
3	electrode	0.01 thick	Al
4	cryopanel	0.1 thick	18 vol.% Al, 2 vol.% HT-9, 80 vol.% void
5	electrical insulator	0.1 thick	Al_2O_3
6	electrode support structure	0.01 x 0.5 x 1.3	Al
7	vacuum valve	0.15 x 0.51 x 1.3	HT-9
8	vacuum separator	0.01 thick	HT-9 or Al
9	neutralizer	0.03 x 2.5 x 0.75	25 vol.% Al, 75 vol.% void
10	mirror	0.03 x 2.5 x 0.03	75 vol.% Mo, 25 vol.% H_2O
11	ion sources	see Fig. 9	
12	magnetic shield and vacuum vessel	0.02 thick each	Al
13	flux trap	0.1 x 0.2 x 1.3	void
14	W-shield	~ 0.75 x 1.22 x 1.75	80 vol.% W, 10 vol.% 304-SS, 10 vol.% H_2O
15	B_4C-shield	~ 0.05 thick	8 vol.% B_4C, 10 vol.% 304-SS, 82 vol.% H_2O
16	boral lining	0.01 thick	36.6 vol.% B_4C, 63.4 vol.% Al
17	water layer	0.2 thick	90 vol.% H_2O, 10 vol.% 304-SS
18	shield	0.2 thick	65.4 vol.% 304-SS, 29.2 vol.% H_2O, 2.1 vol.% B_4C, 3.3 vol.% Pb

magnetic fields.[13] Alumina (Al_2O_3) is used as the high-voltage insulator in the NBI. It is a well developed ceramic insulator and can tolerate[14] a neutron fluence up to 5×10^{24} n/m^2 ($E_n > 0.1$ MeV).

3.4 Penetration Shield Design

Special attention was paid to the design of the NBI shield as the amount of radiation which leaks through the penetration can be controlled to some extent by proper choice of material, composition, and arrangement of the radiation shields. To effectively attenuate the streaming radiation, tungsten is used to surround the double-bend penetration at the HEBT section. The W-shield [80 vol.% W (90% d.f.), 10 vol.% 304-SS, and 10 vol.% H_2O] which is effective in slowing down the high energy neutrons, is backed by several centimeters of B_4C-shield [8 vol.% B_4C (87% d.f.), 10 vol.% 304-SS, and 82 vol.% H_2O] to further moderate the neutrons and absorb the low energy neutrons. The promising results of other studies[5,15,16] suggested the installation of a flux trap, designated 13 in Fig. 10, in the W-shield to improve the attenuation by trapping most of the particles streaming up the straight beam duct. Boral (B_4C and Al) as a penetration shielding material was found[5] to reduce the thermal group flux around the penetration by two to three orders of magnitude, and is recommended as a duct lining material for penetrations. In this regard, the NBI penetration is completely lined with 0.01 m boral sheets. Normally the beam duct is lined with an electrical conductor to avoid the buildup of surface charges. Since boral is a conductor, it is not expected to cause any problem in this regard. However, the outgassing and vacuum properties of the boral in this position need to be examined.

In the region surrounding the straight beam duct, the expensive W-shield was avoided in favor of a less effective lower cost shield since space utilization is not a constraint. The shield there is made of two layers, each 0.2 m thick. The first layer is mainly water with 10 vol.% structural content. The water is almost transparent for the high energy neutrons but it is a good moderator in the intermediate energy range. Therefore, the water layer reduces the backscattering into the penetration by providing a relatively clear path for the energetic neutrons and thermalizing the lower energy neutrons. In addition, the water layer offers the advantage of easily draining the water from the containing tank for easy personnel access to the laser neutralizer for maintenance, adjustment, or replacement. The radiation leaked from the water layer is intercepted by a 0.2 m thick layer made of a homogeneous mixture of the magnet radiation shield used in the end cell. Admittedly, extra shield can be added if the shield thickness is not sufficient to reduce the biological dose to an acceptable level.

3.5 Calculational Procedures and Results

The model shown in Fig. 10 was entered into the MCNP input to treat the problem of the radiation effects on the NBI components. The material cross sections were taken from the RMCCS library based on the ENDF/B-V evaluation.[8] The problem employs neutron and gamma ray surface sources at the duct entrance of 2.204×10^{16} and 3.75×10^{15} particles/s, respectively, as obtained from the previous model of the end cell shield and penetrations (Section 2). The source particles are sampled according to their energy distributions given in Figs. 6 and 7. To improve the statistical accuracy of the results, the source angular distribution, shown in Figs. 6 and 7, was

biased toward the injector axis by sampling from biased cumulative distribution functions and adjusting the weights of the source particles to reflect this effect. Particle transport through the NBI relied heavily on geometry splitting coupled with the Russian Roulette variance reduction technique.[8]

To evaluate the effectiveness of the flux trap and the arrangement of shielding for the straight beam duct, the perturbation version of the MCNP code was utilized. The current version handles a maximum of two perturbed problems simultaneously; the use of this version has the advantage that particle histories are correlated and the computation effort is typically less than that required for independent calculations. The geometric perturbation is treated by changing the material and/or densities in the desired perturbed geometry. For instance, to evaluate the effect of the flux trap, all histories are followed once with the exception that for particles entering the flux trap the history is followed twice: once with void in the flux trap, and once with this region filled with the W-shield. A similar treatment is carried out for the second perturbed problem where the consequences of placing a water layer in the straight beam duct were investigated, in comparison to filling this layer with shielding material.

The 100,000 histories run of MCNP results in the neutron fluxes at several components of the NBI. The flux at the ion source is as low as $10^5(\pm 50\%)$ n/cm^2 s. Since the flux at the duct entrance is $\sim 10^{13}$ n/cm^2 s, we conclude that a neutron attenuation of about eight orders of magnitude is achieved. This is mainly attributed to the design of a narrow and bent beam channel through the $\sim$ 0.7 m thick W/B_4C shield, in addition to the $1/r^2$ geometrical attenuation of the flux. It is worth mentioning that each bend attenuates the streaming radiation through the double-bend penetration by about an

order of magnitude. This was evident by examining the current across surfaces located at the beginning and end of each bend. The shield surrounding the double-bend helps attenuate the high energy neutrons and the neutrons at the accelerator and ion sources have energies below 1 MeV.

The MCNP results indicate a reduction of up to 45% in the neutrons back-scattered from the shield wall of the straight beam duct in the case of water filling the front 0.2 m of the shield. About 40% reduction in the number of neutrons crossing a surface located at the end of the double-bend was obtained as a result of using the flux trap and an even greater reduction of 65% was achieved in the case of using the water layer in the shield of the straight duct. Evidently the installation of the flux trap and the water layer substantially reduces the streaming radiation beyond the double-bend penetration.

The computations also include some results of interest. The first insulating support of the electrodes in the double bend penetration has the highest neutron fluence of $10^{22}(\pm 15\%)$ n/m^2 ($E_n > 0.1$ MeV) compared to the other insulators. It appears that the alumina insulator would last the 24 FPY reactor life as far as radiation is concerned. If the MACOR[17] insulator is prefered because of its machinability, it can still be used without any expected problems during the reactor life although it tolerates a relatively lower fluence level[2] of $\sim 5 \times 10^{22}$ n/m^2. The nuclear heat loads on the cryopanels and magnetic shield seem acceptable with maximum values of $0.023(\pm 8\%)$ and $0.012(\pm 10\%)$ mW per cm^3 of the solid material, respectively, which are not expected to cause an excessive cryogenic load. The volumetric heating rate in the laser neutralizer mirror is $0.03(\pm 45\%)$ mW/cm^3 and may not need additional cooling except as required for the removal of the heat resulting from the surface absorption of the laser beam.

The activation analyses were carried out using the DKR code[18] and its data library. The analyses employ the neutron fluxes and energy spectra at every material zone as obtained from the previous MCNP run. The analyses result in the decay gamma rays at each component in the NBI at the end of a 1 FPY irradiation period and a cooling-off period of 2 days after shutdown. The analyses show that the decay gamma photons have energies below 3 MeV and are emitted at a rate ranging from $\sim 7 \times 10^{11}$ γ/s in the regions adjacent to the NBI entrance to < 0.5 γ/s at the back of the injector.

The activation analyses were followed by a final run of MCNP which included the transport calculations of the gamma rays and the computation of the biological dose rate at various locations outside the NBI. Enough histories were run to ensure that the statistical uncertainty in the dose at the ion sources was less than 10%. The results are reported in Table 4 and the gamma flux-to-dose conversion factors were taken from Ref. 8 (Appendix G). The biological dose at the ion source is ~ 0.1 mrem/h two days after shutdown. This is well below the limit and it is now assured that the routine maintenance of the ion sources can be completed in a hands-on fashion rather than remotely. However, the radiation level elsewhere around the NBI is quite high and to reduce it to an acceptable level additional Pb-shield (a good gamma absorber) is required especially near the duct entrance. On the basis of ~ 0.1 m of Pb-shield reducing the flux by an order of magnitude, the estimated shield thicknesses needed are 0.3, 0.2, and 0.1 m at the regions designated I, (F,J), and (D,G,H) in Fig. 10, respectively.

4. RADIATION ANALYSES FOR THE DIRECT CONVERTOR

Tandem mirror reactors require a large amount of recirculating power; the ability of the direct convertor (DC) to supply most (or all) of this power has the advantage of increasing the overall plant efficiency. Moreover, since this power becomes available as soon as fusion takes place, it can supply power for startup before the turbines begin generating electricity. The end plasma technology is aimed at directly recovering as much energy as possible from the charged particles leaking from the hot core plasma and the cold halo region. The imperfect end plug confinement results in substantial leakage of charged particles from the central cell core plasma out the ends where they are collected on the inner and outer collectors and halo scraper. The halo plasma near the wall is not confined by the potential peaks in the end cells and is free to stream into the end tank where it is collected on the halo scraper. The direct conversion is accomplished by electrically separating the inner/outer collector plates from the halo scrapers. The direct energy recovery system consists of similar components at both ends of the reactor.

The MARS design uses a new compact, gridless direct convertor which fits within the vacuum vessel of the end cell as depicted in Fig. 11. As expected, the charged particles must be collected on surfaces designed to accept high heat fluxes (200-300 W/cm^2) without significant radiation damage. Also, the requirements for high water temperature (320°C) with high flow rate (>10 m/s) and low tritium permeation in the cooling water system forced consideration of the molybdenum alloy TZM as a candidate material for the DC collector plates and halo scrapers. However, the long lived activation products of molybdenum and the waste disposal of the collector plates caused some concern. This brought the need for neutronics and activation analysis for the

Table 4. Biological dose rate around the NBI at the end of one full power year irradiation period and two days after reactor shutdown.

Region*	Dose Rate (mrem/h)
A	0.088 (± 4%)
B	0.038 (± 7%)
C	0.183 (± 10%)
D	30.75 (± 15%)
E	3.98 (± 30%)
F	130.27 (± 15%)
G	12.42 (± 16%)
H	17.06 (± 32%)
I	2.17×10^3 (± 6%)
J	3.41×10^2 (± 20%)

*See Fig. 10

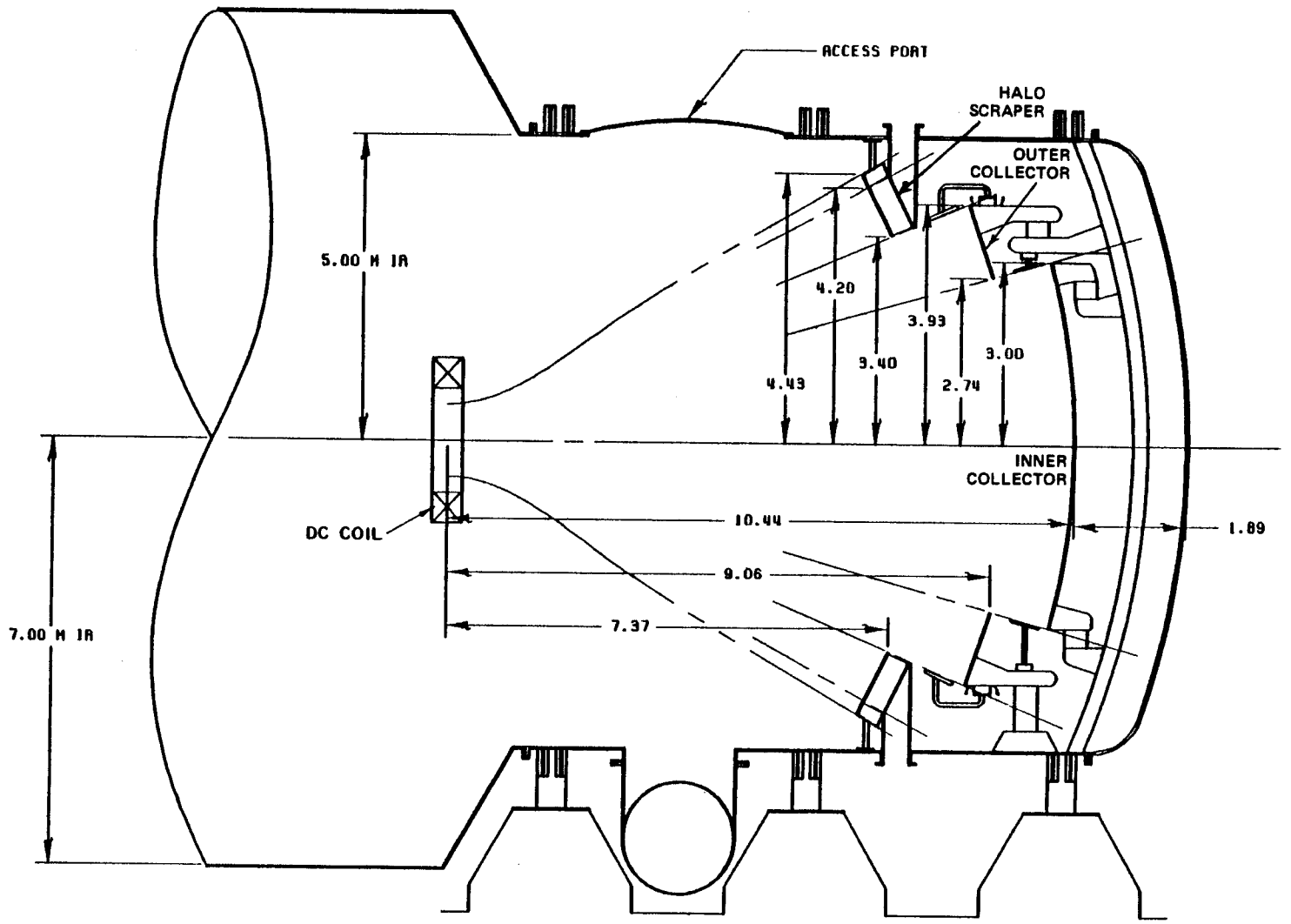

Fig. 11 MARS end plasma system.

DC collector plates to investigate the possibility of simple disposal of the radioactive waste.

4.1 Neutronics Analyses

The problem of neutron streaming from the reaction chamber to the direct convertor region was analyzed using the Monte Carlo code MCNP.[8] The calculational model is a duplicate of the model used in the streaming study of the end cell penetrations (Section 2). The neutron source, given in Fig. 3, was modeled from the midplane of the choke coil to the end of the plug region and sampled within the plasma boundary. To reduce the statistical error, the isotropic neutron source was directionally biased toward the direct convertor and the neutron weights were adjusted to reflect this variance reduction procedure. The homogeneous mixture used for the DC collector plates consisted of 95.5 vol.% molybdenum and 4.5 vol.% water. A run was made using 30,000 histories and the results were normalized to a total source of 7×10^{18} n/s. The calculations show that the values of the neutron fluxes at the inner collector, outer collector, and halo scraper are 5.09×10^{9} (± 7%), 4.78×10^{8} (± 12%), and 3.33×10^{8} (± 13%) n/cm^2 s, respectively. As anticipated, the inner collector has the highest flux as other plates are shielded from the direct neutron source. Editing of the results made use of the segmentation feature of MCNP. The 3 m radius inner collector plate was divided radially into 30 segments, each 0.1 m thick. The flux in each segment was printed and a plot of the results is given in Fig. 12. The flux peaks at the center of

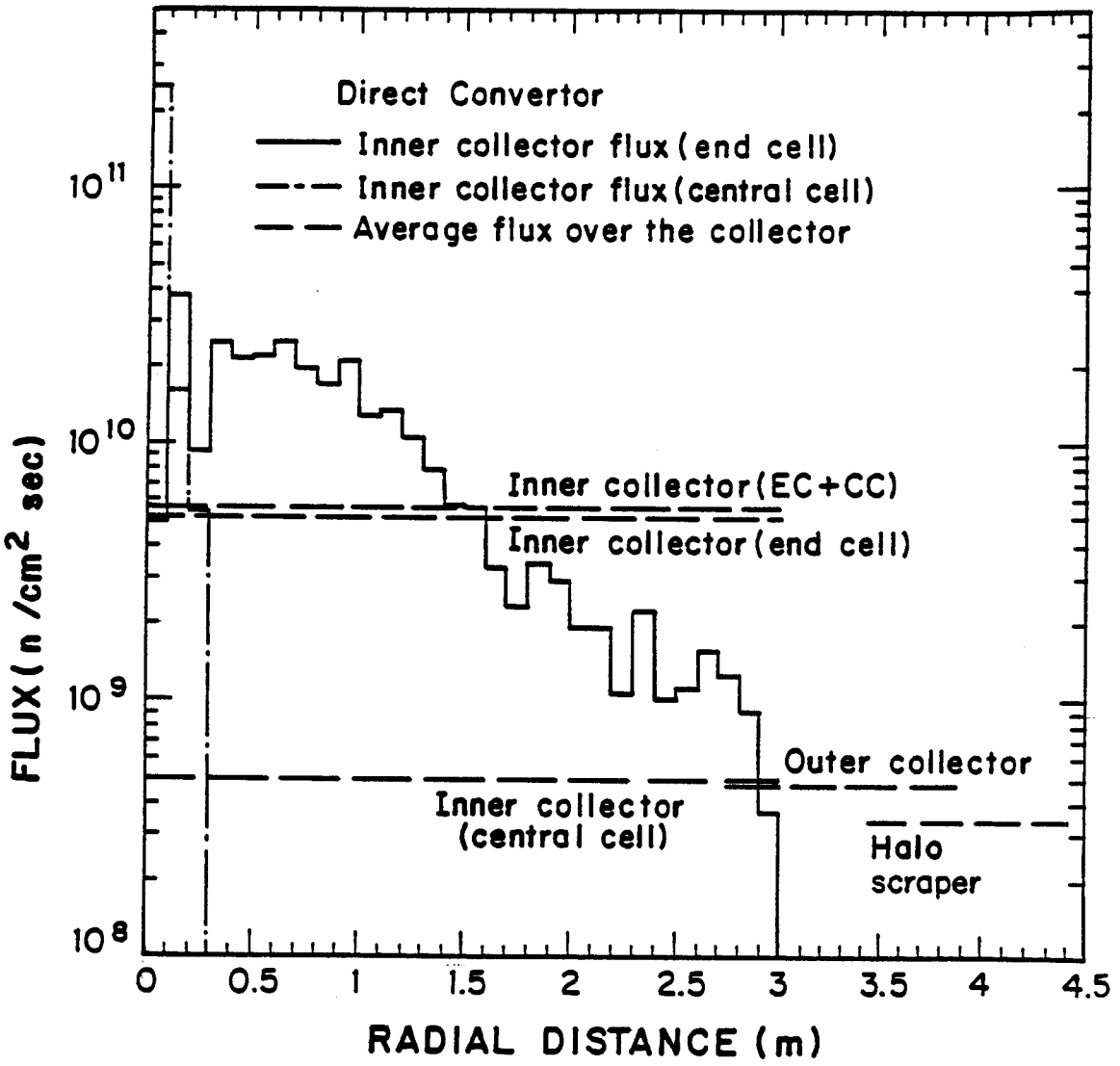

Fig. 12 Neutron flux at the direct convertor collector plates.

the plate and drops off radially toward the edge. The energy distribution of the neutron flux was also obtained and is presented in Fig. 13.

An attempt was made to analytically calculate the DC flux due to neutron streaming from the central cell based on several assumptions: 1) the neutron source is uniform across the plasma cross section; 2) only source neutrons are able to reach the DC as the choke coils attenuate the secondary neutrons generated in the blanket; and 3) the amount of neutron streaming into the DC is determined by the dimensions of the shield walls at the first two plasma fans closest to the central cell. The analytical results have shown that the average 14.1 MeV neutron flux over the inner collector plate is 4.94×10^8 n/cm^2 s. The estimated radial distribution of this flux is shown in Fig. 12. This leads to a total flux at the inner collector plate of 5.59×10^9 n/cm^2 s.

4.2 Activation Analyses

The activation analyses were carried out for the DC plates using the DKR[18] fusion reactor radioactivity calculation code and its associated data library. The analyses employ the neutron fluxes and energy spectra obtained from the MCNP run as described before. Two cases were considered with irradiation times of 12 and 24 FPY's and the results are given in Tables 5 and 6. The legal limits in these tables are taken from 10CFR61[19] or estimated from the data therein. The Waste Disposal Rating (WDR) serves as a guide to the designers in evaluating how easily a particular material can be disposed of. The WDR is the sum of the ratio of the specific activity to the maximum permissible concentration for the different isotopes. If the WDR>1, the material cannot be disposed of by near surface burial unless diluted. If $0.1 < WDR < 1$,

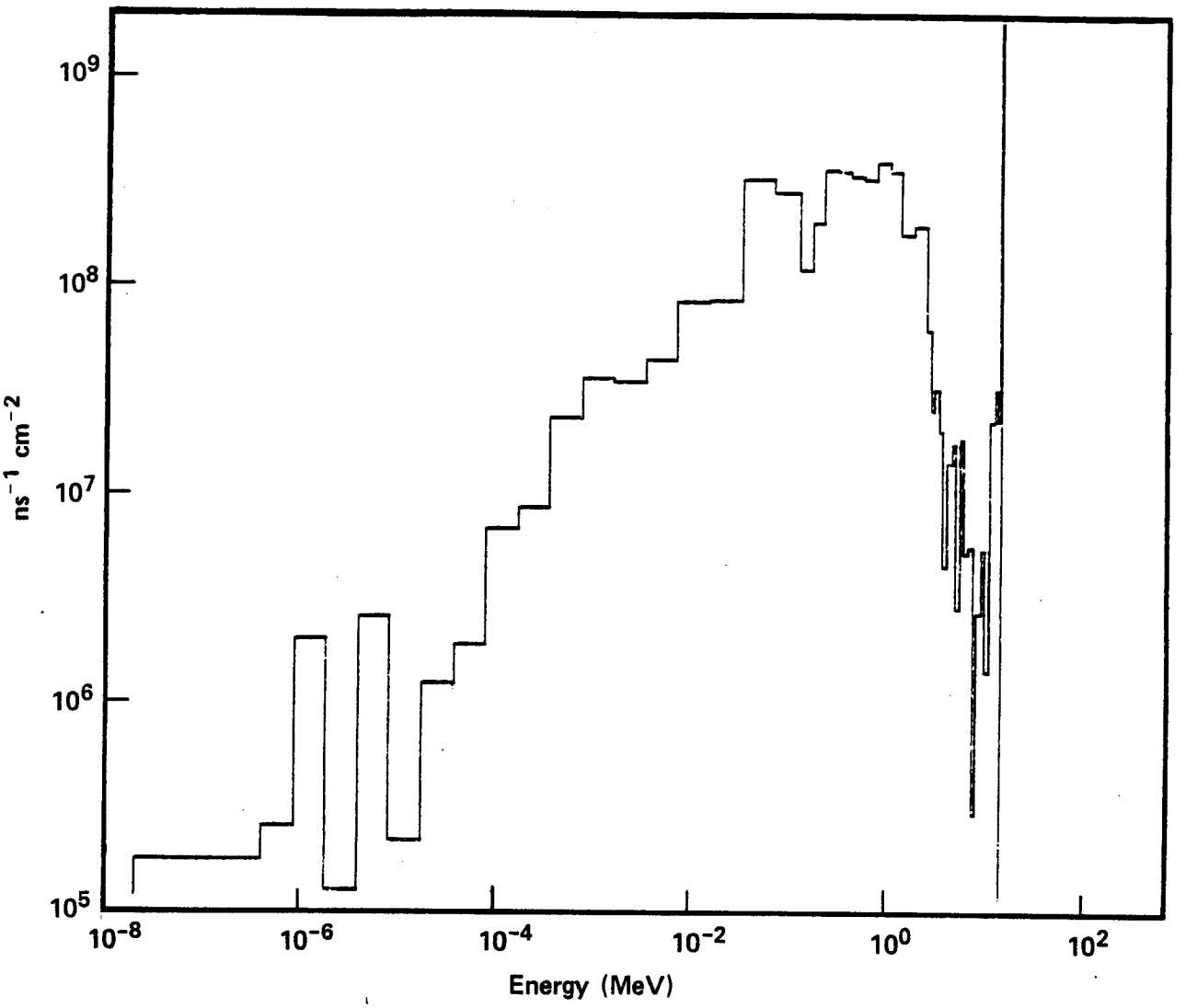

Fig. 13 Neutron energy spectrum for the inner collector plate.

Table 5. Specific activities for direct convertor (Ci/m^3) - 12 FPY irradiation time.

Isotope	Inner collector	Outer collector	Halo scraper	Class C legal limit	Fraction of legal limit
^{93}Mo	6.53×10^{0}	5.25×10^{-1}	3.72×10^{-1}	220	0.029
^{94}Nb	7.50×10^{-3}	2.13×10^{-5}	3.54×10^{-5}	0.2	.0375
^{99}Tc	5.20×10^{-3}	8.74×10^{-4}	6.61×10^{-4}	3	.0015
					WDR = .068

Table 6. Specific activities for direct convertor (Ci/m^3) - 24 FPY irradiation time.

Isotope	Inner collector	Outer collector	Halo scraper	Class C legal limit	Fraction of legal limit
^{93}Mo	1.31×10^{1}	1.05×10^{0}	7.41×10^{-1}	220	0.059
^{94}Nb	1.5×10^{-2}	4.25×10^{-5}	7.07×10^{-5}	0.2	.075
^{99}Tc	1.04×10^{-2}	1.75×10^{-3}	1.33×10^{-3}	3	.003
					WDR = .137

the waste is termed low level Class C intruder waste. This waste must be packaged for near surface burial with the idea that it will still pose a hazard after the 100 year institutional period is over. If WDR < 0.1, the waste is Class A segregated waste. It must meet less stringent packaging and burial requirements.

Tabulated results show that the DC plates could be classified as Class A waste in the case of 12 FPY irradiation period and Class C for the 24 FPY period. However, in the latter case the waste could easily be converted to Class A by encasing the plates in concrete and increasing its volume by f 40%. Alternatively, the central portion of the inner collector could be removed and buried as Class C waste with the remainder of the inner collector, the outer collector, and the halo scraper disposed of as Class A.

5. Conclusions

The MARS end cell was modeled for radiation streaming analysis using the Monte Carlo code MCNP. The calculations result in the amount of radiation at the penetration entrances and the neutron flux at the direct convertor collector plates. The inner collector has the highest flux of 5.6×10^9 n/cm^{2}s, as the other plates are shielded from the direct neutron source. The subsequent activation analyses reveal that near surface burial of the DC collector plates is feasible. It is noteworthy that the neutron flux at the DC collector plates is relatively low so that bulk damage that is normally associated with such neutrons is probably not important but the sputtering problems of the energetic charged particles could be adverse unless properly handled.

The results indicated that the NBI duct has the highest energy current density (0.06 MW/m^2) at the entrance and this could be a source of difficulty unless additional shielding is introduced within the injector. On this basis, bends were provided in the penetration to facilitate shielding and reduce streaming. The 3-D neutronics and activation analyses of the NBI show that the biological dose rate at the back of the injector is reasonably low so that some of the routine maintenance of the ion sources can be completed in a hands-on procedure. This is mainly attributed to the combined effect of choosing low activation materials in the NBI and the off-axis arrangement of the ion sources and the transmission system which was designed to be compatible with the bends. The analyses also indicate that the nuclear heat loads on the various components are not expected to cause any problems and the electrical insulators will last the reactor life as far as radiation is concerned.

While there is no problem with the NBI of the MARS design, it could become a problem in reactors with high entrance wall loadings such as tokamaks where the incident radiation is about two orders of magnitude higher. The designer will then have to provide either more bends in the penetration shield, or maintain the ion sources in a remote fashion.

Acknowledgements

The author wishes to acknowledge helpful discussions with Professors Charles Maynard and William Vogelsang of the University of Wisconsin. She is also grateful to Andrew White for his assistance with the radioactivity calculations. This work was performed under the auspices of the United States Department of Energy.

References

1. M.M. Ragheb and C.W. Maynard, "Neutronics Shielding Analysis for the End Plug of a Tandem Mirror Fusion Reactor," Journal of Fusion Energy 1, 367 (1981).

2. L.A. El-Guebaly and C. Maynard, "Radiation Streaming in Penetrations of TASKA", Nuclear Technology/Fusion, 5, 101 (1984).

3. R.A. Lillie, R.T. Santoro, and R.G. Alsmiller, Jr., "Estimated Nuclear Effects in the Neutral Beam Injectors of a Large Fusion Reactor," Oak Ridge National Laboratory Report ORNL/TM-7526 (1980).

4. W.T. Urban, "Neutron Streaming Through Straight and Single Bend Slots", Los Alamos National Laboratory Report LA-9761-MS (1983).

5. M.M. Ragheb, A.C. Klein, and C.W. Maynard, "Neutronics Shielding Analysis of the Last Mirror-Beam Duct System For a Laser Fusion Power Reactor", Nuclear Technology/Fusion, 1, 99 (1981).

6. B.G. Logan et al., "Mirror Advanced Reactor Study - Final Report", Lawrence Livermore National Laboratory Report, UCRL-53480 (1984).

7. B.G. Logan et al., "Summary of the Mirror Advanced Reactor Study," IAEA 10th International Conference on Plasma Physics and Controlled Nuclear Fusion Research, London, England, Sept. 1984.

8. Los Alamos National Laboratory Group X-6, "MCNP - A General Monte Carlo Code for Neutron and Photon Transport, Version - 2C," Los Alamos National Laboratory Report LA-7397-M (1981).

9. K.N. Leung and K.W. Ehlers, "LBL Self-Extraction Negative Ion Source", Lawrence Berkeley Laboratory Report LBL-13261 (1981).

10. W.S. Cooper, "Summary of the Status of Negative-Ion-Based Neutral Beams", Proc. of 5th Topical Meeting on the Technology of Fusion Energy, Knoxville, Tennessee (1983).

11. W.F. Vogelsang, University of Wisconsin, Private Communication.

12. D.W. Dorn and R.C. Maninger, "Issues in Radioactivity for Fusion Energy Remote-Maintenance Rating", Lawrence Livermore National Laboratory Report UCRL-89195 (1983).

13. K.W. Ehlers, Lawrence Berkeley Laboratory, Private Communication.

14. L.A. El-Guebaly, "Material Considerations for ICRF Ceramic-Filled Waveguide Launchers", University of Wisconsin Fusion Technology Institute report, UWFDM-579, Aug. 1984.

15. B.A. Engholm, J.M. Battaglia, and J.F. Baur, "Radiation Streaming in Diagnostic Penetrations", Proceedings of the 6th International Conference on Radiation Shieldings, Tokyo, Japan (1983).

16. X. de Seynes, "Shielding Conditions for Neutral Beam Injection Systems", Thesis for Degree of Master of Engineering, University of California, Berkeley (1983).

17. MACOR is a product of the Corning Glass Works, Corning, N.Y.

18. T.Y. Sung and W.F. Vogelsang, "DKR: A Radioactivity Calculation Code for Fusion Reactors", University of Wisconsin Fusion Engineering Program Report, UWFDM-170 (1976).

19. Code of Federal Regulation, "Licensing Requirements for Land Disposal of Radioactive Wastes", Vol. 47, #248, Chapter 10 (1982).